

EXPRESS LETTER

Ductile compaction of partially molten rocks: the effect of non-linear viscous rheology on instability and segregation

E. Veveakis,^{1,2} K. Regenauer-Lieb^{2,3} and R.F. Weinberg⁴

¹*CSIRO Earth science and Resource Engineering, 26 Dick Perry Ave., Kensington, WA 6151, Australia. E-mail: manolis.veveakis@csiro.au*

²*School of Petroleum Engineering, University of New South Wales, Sydney, NSW, Australia*

³*School of Earth and Environment, The University of Western Australia, Crawley, WA, Australia*

⁴*School of Geosciences, Monash University, Clayton, Victoria, Australia*

Accepted 2014 October 20. Received 2014 October 17; in original form 2014 June 19

SUMMARY

The segregation of melt from a linear viscous matrix is traditionally described by McKenzie's compaction theory. This classical solution overlooks instabilities that arise when non-linear solid matrix behaviour is considered. Here we report a closed form 1-D solution obtained by extending McKenzie's theory to non-linear matrix behaviours. The new solution provides periodic stress singularities, acting as high porosity melt channels, to be the fundamental response of the compacted matrix. The characteristic length controlling the periodicity is still McKenzie's compaction length δ_c , adjusted for non-linear rheologies.

Key words: Geomechanics; Creep and deformation; Mechanics, theory, and modelling.

1 INTRODUCTION

Melt segregation is found to be an extremely efficient mechanism capable of squeezing even small fractions of melt out of the solid rock matrix through localized channels (McKenzie 1985; Connolly *et al.* 2009). Following the pioneering work of McKenzie (1984), the classical interpretation is that they are features of gravity driven volumetric compaction of a linear viscous matrix with the melt migrating through the matrix in small portions via grain boundary wetting. It was therefore identified to be a process predominantly controlled by the properties of the melt, with the solid contributing by its dihedral angle to determine whether melt migrates through the linear viscous matrix. The problem remained that the classical solution does not localize and consequently the melt velocities on the grain boundaries were significantly smaller than inferred from field observations (Brown *et al.* 1995; Team 1998). The volumetric compaction of the solid matrix therefore appeared not to be the source of the instabilities and shear induced failure modes were promoted (Holtzman *et al.* 2003a; Katz *et al.* 2006; Kohlstedt & Holtzman 2009). In this work we present a fundamental yet so far overlooked—instability process that is driven predominantly by the solid matrix instead of the gravity driven percolation flow of linear melt through the solid matrix. This process therefore belongs to the class of solid material instabilities that are caused by an applied stress field.

Based on laboratory experiments shear-induced dilatant instabilities at low angles to σ_1 as shown in Fig 1(a) were argued to be the most efficient mechanism to explain the necessary localization and speed of melt transport (Holtzman *et al.* 2003a,b; Kohlstedt & Holtzman 2009). Theoretical and numerical approaches were developed in parallel with these experimental observations of localized

melt segregation instabilities (Scott & Stevenson 1984; Stevenson 1989; Connolly & Podladchikov 1998, 2007; Spiegelman *et al.* 2001; Rabinowicz & Vigneresse 2004; Katz *et al.* 2006). All these works emphasized the existence of localized segregation instabilities that can initiate from porosity perturbations in Darcy's law or through an indirect feedback mechanism creating a non-linear (in porosity) viscous response through the porosity variations.

In the field, another alignment of the instabilities can also be encountered. They can be found at high angles to the maximum principal stress direction, a regime that can be met in both shear-induced (Fig. 1b; Weinberg *et al.* 2013) and purely volumetric cases (Fig. 1c; Vernon & Paterson 2001; Weinberg & Mark 2008). These observations highlight the existence of a volumetric failure mode at the high confining pressures encountered in the middle to lower crust, in addition to the above described failure modes and McKenzie's pervasive solution of melt transfer. In this work, we emphasize on this regime and seek for the predominant mechanisms controlling the problem of volumetric compression of partially molten rocks. We seek for fundamental types of volumetric material failure that emerge from a homogenous porosity and deformation states. We therefore provide a simple extension of McKenzie's compaction theory and show that volumetrically induced melt segregation instabilities are a fundamental poro-mechanical response of a solid matrix with non-linear rheology.

2 MODEL FORMULATION

We consider a 1-D model formulation based on the method of characteristics developed in the general theory of plasticity (Hill 1950). This method reduces a generalized geometrical problem in

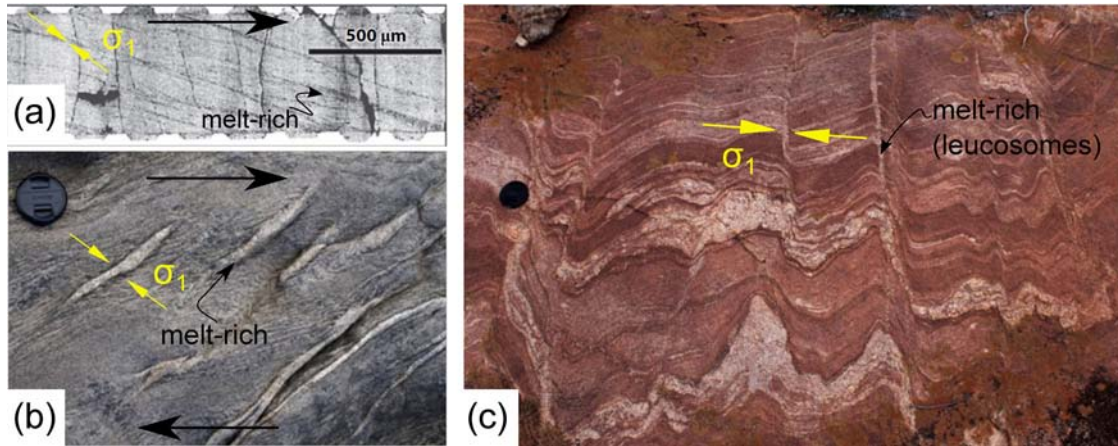


Figure 1. Melt-rich channels at different settings. (a) Figure from laboratory experiments, after Holtzman *et al.* (2003a,b), showing melt-rich channels forming during shear at low angles with respect to the maximum compressive stress (yellow arrows). (b) Outcrop from Kangaroo Island, Australia (Weinberg *et al.* 2013) showing melt-channels forming under shear, with the orientation of the melt-rich bands (leucosomes) at high angles to (a) under a similar maximum compressive stress orientation. (c) Banded and folded ductile Archean gneiss with layer-parallel pegmatite intrusions (horizontal white bands). Folds have axial planar leucosomes (crystallized melt) oriented N–S across the photograph. These melt channels form at high angle to the maximum compressive stress (yellow arrows), oriented E–W. The orientation of the maximum compressive stress is inferred by the folding patterns and lacking evidence for high pore pressures such as generalized brittle fracturing filled with leucosomes. Note the 20–50 cm spacing between leucosome (melt channels) bands of 10 mm thickness. Outcrop from the Yalgoo Dome, Yilgarn Craton and West Australia.

two dimensions into an equivalent 1-D failure line along a marching coordinate system ξ . These failure lines are constructed in a stress space that allows a decomposition of purely volumetric and purely deviatoric components acting across and along them, respectively. In oedometric conditions for example (where in an $x-y-z$ Cartesian coordinate system $\epsilon_{xx} = \epsilon_{yy} = 0$ and $\epsilon_{zz} \neq 0$), the direction of ξ coincides with the purely compactive/dilatational z -direction.

In this contribution, we investigate the influence of the volumetric mechanism acting along the axis normal to the instability (ξ) and solve for the distribution of the mean effective stress p' inside the compressed specimen of height $2H$, defined as the area that reaches the yield stress. For mathematical simplicity, we assume that all material properties, including solid viscosity and permeability, are constant. This restricts the validity of the approach to the onset of instability and the emergence of volumetric localization from homogeneous deformation. Rather than developing solutions for transient elasto-viscoplastic wave propagation we seek for the stationary wave manifestation of the system because this solution corresponds to the fundamental eigenmodes of the system to which all transients relax (Hill 1962).

2.1 Momentum and mass balance

Based on this approach we position ourselves in the plastified area $2H$ where the initial elasto-plastic loading has occurred and therefore all the stress quantities are exceeding the yield regime, in a classical setting of overstress viscoplasticity (Perzyna 1966). Stress equilibrium in the ξ -direction combined with the stress decomposition $p = p' + p_f$ (p_f is the pressure of the fluid/melt and p' is the mean effective stress) provides

$$\frac{\partial p'}{\partial \xi} = \frac{\partial p_f}{\partial \xi}. \quad (1)$$

In the bi-phasic setting considered, we define the partial densities $\rho^{(1)} = (1 - \phi)\rho_s$ and $\rho^{(2)} = \phi\rho_f$ of the solid and melt/fluid phase, respectively, ϕ being the porosity (melt/fluid content), ρ_s and ρ_f the solid skeleton and melt/fluid density, respectively. The mass

balance for each of the phases is $\frac{\partial \rho^{(a)}}{\partial t} + \frac{\partial \rho^{(a)} v_\xi^{(a)}}{\partial \xi} = 0$, where $a = 1, 2$ are superscripts for the solid and melt/fluid phase, respectively. Following McKenzie's approach for incompressible solid and fluid (i.e. $\rho_s, \rho_f = \text{const.}$), the mass balance equation for each of the phases reduces to:

$$-\frac{\partial \phi}{\partial t} - \frac{\partial \phi v_\xi^{(1)}}{\partial \xi} + \frac{\partial v_\xi^{(1)}}{\partial \xi} = 0, \quad (2)$$

$$\frac{\partial \phi}{\partial t} + \frac{\partial \phi v_\xi^{(2)}}{\partial \xi} = 0. \quad (3)$$

By adding them we obtain the mixture's mass balance equation

$$\frac{\partial \phi (v_\xi^{(2)} - v_\xi^{(1)})}{\partial \xi} + \frac{\partial v_\xi^{(1)}}{\partial \xi} = 0. \quad (4)$$

As in McKenzie's approach we accept Darcy's law for the separation velocity $\phi (v_\xi^{(2)} - v_\xi^{(1)})$,

$$\phi (v_\xi^{(2)} - v_\xi^{(1)}) = -\frac{k_\pi}{\mu_f} \frac{\partial p_f}{\partial \xi}, \quad (5)$$

where k_π is the constant permeability, and μ_f the fluid viscosity.

The volumetric strain rate is defined as $\dot{\epsilon}_V = \frac{\partial v_\xi^{(1)}}{\partial \xi}$. Under these considerations, and by considering constant permeability, we obtain (Vardoulakis & Sulem 1995),

$$\frac{k_\pi}{\mu_f} \frac{\partial^2 p_f}{\partial \xi^2} = \dot{\epsilon}_V. \quad (6)$$

2.2 Non-linear viscous case

In this study, we restrict our discussion to the case where the solid matrix can receive the stresses and the overall bulk behaviour is that of a solid. The considered scale for this solid mechanical problem is the timescale of melt segregation which is of the orders of years and not the timescale of geodynamic deformation. Therefore the matrix support is defined by the interacting solid skeleton and not the

percolating melt network. A complete solution to the problem considers the strain rate to be decomposed into elastic and viscoplastic components and makes it necessary to calculate the elastic transients of the stress and porosity wave propagation. Following the classical approach of material bifurcation (Hill 1962) we solve for the stationary attractor of this elasto-viscoplastic problem (i.e. the limit of rigid viscoplastic material) and investigate the response of the matrix to volumetric deformation. To this end a standard power law rheology relating the strain rates with the effective stress can be assigned (see, e.g. Hickman & Gutierrez 2007; Oka *et al.* 2011, and references therein):

$$\dot{\epsilon}_V = \dot{\epsilon}_n \left[\frac{p'}{p'_n} \right]^m, \quad (7)$$

where $\dot{\epsilon}_n$ is the creep parameter (in s^{-1}) and p'_n a reference stress-like quantity. In their constitutive work, Hickman & Gutierrez (2007) evaluated the material parameters $\dot{\epsilon}_n$ and m as functions of the porosity and the slopes of the compression curves in isotropic compression tests. This means that $\dot{\epsilon}_n$ (here kept constant for simplicity) is in principle a function of all the state variables of the problem, thus varying with porosity and temperature changes (see also the work of Rabinowicz & Vigneresse (2004)). In this work $\dot{\epsilon}_n$ is set to be the loading strain rate at the boundary where equivalent loading p'_n is applied.

Eq. (7) is the volumetric component of the flow law that is frequently used in describing shear deformation and was introduced here following the current practice in the mechanics of soft geomaterials (Hickman & Gutierrez 2007; Oka *et al.* 2011) to illustrate the rate dependent deformation of purely volumetric nature. Note that the kinematic quantities $\dot{\epsilon}_n$ and $\dot{\epsilon}_V$, as well as the static fields p' and p'_n must always have the same sign, in order to ensure positive mechanical work and satisfy the second law of thermodynamics. This means that the present formulation is invariant of the sign convention of the static and kinematic fields and applies to purely volumetric compaction and dilatational problems.

3 MATHEMATICAL CONSIDERATIONS

By combining eqs (1), (6) and (7), we obtain

$$\frac{k_\pi}{\mu_f} \frac{\partial^2 p'}{\partial \xi^2} = \dot{\epsilon}_n \left[\frac{p'}{p'_n} \right]^m. \quad (8)$$

The final eq. (8) is brought into a dimensionless form:

$$\frac{d^2 \sigma'}{dz^2} - \lambda \sigma'^m = 0, \quad (9)$$

by considering $z = \frac{\xi}{H}$, $\sigma' = \frac{p'}{p'_n}$ and

$$\lambda = \frac{\dot{\epsilon}_n \mu_f}{k_\pi p'_n} H^2 = \left(\frac{H}{\delta_c} \right)^2. \quad (10)$$

Note that McKenzie's expression (A33) is retrieved for $m = 1$ and that the dimensionless group λ scales with a modified compaction length that includes the adjusted matrix viscosity $\bar{\mu}_s = \frac{p'_n}{\dot{\epsilon}_n}$,

$$\delta_c = \sqrt{\frac{k_\pi \bar{\mu}_s}{\mu_f}}. \quad (11)$$

The solution of eq. (9) depends on the value of the rate sensitivity coefficient m . For $m = 1$ the system degenerates into the classical McKenzie equation without instabilities. For all $m > 1$ (non-linear cases), the solution for σ' is non-trivial, as it is elliptic. For odd values it is the Jacobi and for even values it is the Weierstrass equation

(the two are related, as discussed in Appendix A). This behaviour is frequently met in Korteweg-de Vries equation of the shallow water theory, with the solutions presenting periodic singularities that are spectrally stable (Bottman & Deconinck 2009). This means that the transient orbits of the system are attracted to the solutions of the steady state eq. (9).

For integer values of $m < 4$ this equation admits closed-form solutions (see Appendix A). Without loss of generality we focus in this study on the relevant solutions for a representative power law of $m = 3$ (see also eq. 1a of Rabinowicz & Vigneresse 2004) because this is the most common power law exponent for mantle and crustal rocks. For $m = 3$ and for constant boundary conditions [$\sigma'(1) = 1$ and $\frac{d\sigma'}{dz}|_{z=0} = 0$], the analytic solution of eq. (9) is

$$\sigma' = \pm C_2 sn \left[\left(\sqrt{\frac{-\lambda}{2}} z + \frac{Icn(0, t)}{C_2} \right) C_2, t \right], \quad (12)$$

where sn and Icn are the Jacobi SN and the inverse Jacobi CN function, and C_2 the solution of the transcendental equation $\sigma'(1) = 1$.

4 DUCTILE INSTABILITY CRITERION

The profiles of the normalized effective stress depend on the poromechanical feedback parameter λ . The parameter λ represents the ratio of the mechanical matrix deformation diffusivity over the internal mass diffusive transfer of the melt. This parameter has a profound physical meaning as it states that volumetric instabilities are a result of competition of two time dependent processes, which are the mechanical deformation of the matrix and the internal response of the embedded melt phase. We may anticipate that stable deformation occurs when $\lambda \ll 1$, that is the matrix deformation is much slower than the fluid diffusion rate and the specimen has the time to diffuse away any fluid pressure variations induced by the loading conditions. At the other extreme when $\lambda \gg 1$ the loading rate is much faster than the melt diffusion rate, internal mass variations cannot be equilibrated and coupled poromechanical instabilities are expected.

For $m = 3$ (see Appendix A for other cases), Fig. 2 depicts a complex response, providing a multiplicity of singularities for the normalized effective stress as λ increases. As expected from the above discussed rate competition of diffusion process for small values of λ (approximately $\lambda < 13$) the effective stress profiles present a smooth solution with a minimum at the origin ($z = 0$), as shown in Figs 2(a) and (b).

For values $\lambda > 13$ (see Appendix B for the reasoning) the effective stress presents multiple singularities, the number of which increases with λ . Since these singularities are localized in space, they indicate zones of melt/fluid flow-focus. The following derivation shows that these singularities are high porosity melt channels. This result comes from integrating the mass balance of the solid phase (eq. 2, combined with eq. 7 and neglecting the solid convection) over a reference time interval Δt :

$$\phi = 1 - (1 - \phi_0) e^{-\dot{\epsilon}_n \Delta t \sigma'^m} \quad (13)$$

where ϕ_0 is the initial porosity, considered constant across the sample due to the assumption of homogenous initial state. We emphasize that the porosity is an outcome of this integration, providing a solution of the porosity dependence on the applied stress. In this integration the melt segregation channels emerge as high porosity features out of homogeneous initial porosity. In the limiting case of fully established stress singularities ($\sigma' \rightarrow \infty$) the porosity tends to its maximum value (one) confirming melt segregation instabilities

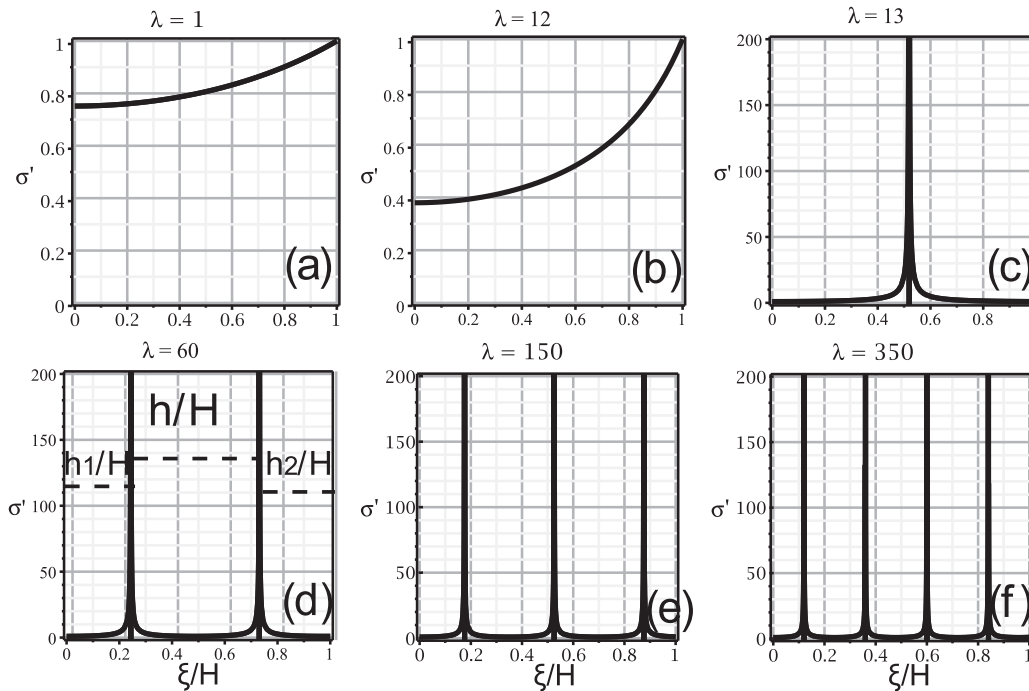


Figure 2. Distribution of the normalized effective stress σ' (eq. 12) inside the specimen for six different values of λ . Although for small values of λ the solution follows the linear case of McKenzie's theory ($m = 1$), stress singularities are obtained for $\lambda > 12$. In (d) the dimensionless distance h/H between the stress singularities in the melt channels is highlighted.

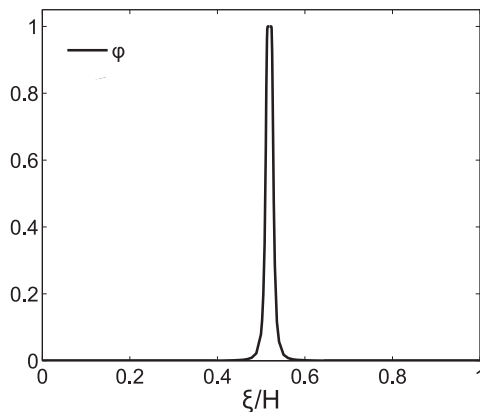


Figure 3. Plot of the porosity profile (eq. 13) for $\lambda = 13$ (see also Fig. 2c) for $\epsilon_n \Delta t = 10^{-5}$ and $\phi_0 = 1$ per cent.

(see Fig. 3). Because these instabilities originate from singularities in the stress distribution of the solid matrix (effective stress), we conclude that they are predominantly solid-controlled features.

A diagnostic element for geological applications in the field is the spacing h between the melt channels as annotated in Fig. 2(d). Although not periodically placed across the specimen, the channels divide the space into equal layers of distance h , since as annotated in Fig. 2(d), $h_1 + h_2 \approx h$. As a consequence, h is then defined as the inverse density of the bands, $h = \frac{H}{N_C}$. Through the results of Fig. 2 we obtain $N_C = 0.27\sqrt{\lambda}$, or

$$h = \frac{H}{N_C} = \frac{\bar{\delta}_c}{0.27} \approx 4\sqrt{k_\pi \frac{\bar{\mu}_s}{\mu_f}}. \quad (14)$$

Field observations of the spacing between the instabilities can be used to verify or estimate material parameters like permeability,

and melt segregation velocities leading to the pattern of Fig. 1(c). For a typical solid tonalite framework with a viscosity of 10^{18} Pa s, a melt viscosity of 10^5 – 10^{10} Pa s and a channel spacing of 50 cm as in Fig. 1(c), we obtain from eq. (14) a realistic range of effective permeability, between 10^{-15} and 10^{-10} m².

5 CONCLUSION

We have presented a non-linear extension of McKenzie's compaction theory, based on the assumption that a solid skeleton is supporting the applied stresses and thus its rheology can be non-linear. We have shown that solid-controlled volumetric instabilities emerge in this process, that are characterized by localized high porosity melt channels that are periodically interspersed inside the compacting matrix. This result suggests that the problem of compaction of partially molten rock can be seen as a fundamental poromechanical response of a non-linear, viscous, partially molten solid matrix. This view of the problem is different than the classical perception of the linear viscous melt driving the process via its percolation through the solid matrix problem. This is because the presented localized mode of volumetric failure stems from a different (short) timescale perspective of melt segregation. On long geodynamic timescales the segregation problem may indeed be seen as a linear viscous melt percolation problem assuming existing pathways for the melt. On the short timescales of the order of years the percolation of solid interacting forces of the solid skeleton define the matrix support. This leads to an overall non-linear viscous behaviour of the system that controls the process of melt segregation. We have shown that in this case a classical solid mechanical approach provides a closed form analytical solution for the steady state attractor of the short timescale porosity waves. In line with the classical bifurcation methods in solid mechanics (Hill 1962) the outcomes of this study are a quasi-static representation of a wave propagation

problem. This does not imply that the reported instabilities take place simultaneously but that the depicted pattern is the end product of an evolution of instabilities as a function of the elasto-viscoplastic (volumetric) p -wave propagation.

REFERENCES

- Abramowitz, M. & Stegun, I., eds, 1964. *Handbook of Mathematical Functions*, U.S. National Bureau of Standards.
- Bottman, N. & Deconinck, B., 2009. KdV cnoidal waves are spectrally stable, *Discrete Contin. Dyn. Syst.*, **25**, 1163–1180.
- Brown, M., Averkin, Y.A., McLellan, E. & Sawyer, E., 1995. Melt segregation in migmatites, *J. geophys. Res.*, **100**(B8), 15 655–15 567.
- Connolly, J., Schmidt, M., Solferino, G. & Bagdassarov, N., 2009. Permeability of asthenospheric mantle and melt extraction rates at mid-ocean ridges, *Nature*, **462**(7270), 209–212.
- Connolly, J.A.D. & Podladchikov, Y.Y., 1998. Compaction-driven fluid flow in viscoelastic rock, *Geodin. Acta*, **11**(2–3), 55–84.
- Connolly, J.A.D. & Podladchikov, Y.Y., 2007. Decompaction weakening and channeling instability in ductile porous media: implications for asthenospheric melt segregation, *J. geophys. Res.: Solid Earth*, **112**, B10205, doi:10.1029/2005JB004213.
- Hickman, R. & Gutierrez, M., 2007. Formulation of three-dimensional rate-dependent constitutive model for chalk and porous rocks, *Int. J. Numer. Anal. Meth. Geomech.*, **31**, 583–605.
- Hill, R., 1950. *The Mathematical Theory of Plasticity*, Oxford Univ. Press.
- Hill, R., 1962. Acceleration waves in solids, *J. Mech. Phys. Solids*, **10**, 1–16.
- Holtzman, B., Groebner, N., Zimmerman, M., Ginsberg, S. & Kohlstedt, D., 2003a. Stress-driven melt segregation in partially molten rocks, *Geochem. Geophys. Geosyst.*, **4**(5), doi:10.1029/2001GC000258.
- Holtzman, B., Kohlstedt, D., Zimmerman, M., Heidelbach, F., Hiraga, T. & Hustoft, J., 2003b. Melt segregation and strain partitioning: implications for seismic anisotropy and mantle flow, *Science*, **301**(5637), 1227–1230.
- Katz, R., Spiegelman, M. & Holtzman, B., 2006. The dynamics of melt and shear localization in partially molten aggregates, *Nature*, **442**, 676–679.
- Kohlstedt, D.L. & Holtzman, B.K., 2009. Shearing melt out of the Earth: an experimentalist's perspective on the influence of deformation on melt extraction, *Ann. Rev. Earth planet. Sci.*, **37**(1), 561–593.
- McKenzie, D., 1984. The generation and compaction of partially molten rocks, *J. Petrol.*, **25**(3), 713–765.
- McKenzie, D., 1985. The extraction of magma from the crust and mantle, *Earth planet. Sci. Lett.*, **74**, 81–91.
- Oka, F., Kimoto, S., Higo, Y., Ohta, H., Sanagawa, T. & Kodaka, T., 2011. An elasto-viscoplastic model for diatomaceous mudstone and numerical simulation of compaction bands, *Int. J. Numer. Anal. Meth. Geomech.*, **35**, 244–263.
- Perzyna, P., 1966. Fundamental problems in viscoplasticity., *Adv. Appl. Mech.*, **9**, 243–377.
- Rabinowicz, M. & Vigneresse, J.-L., 2004. Melt segregation under compaction and shear channeling: application to granitic magma segregation in a continental crust, *J. geophys. Res.*, **109**(B4), doi:10.1029/2002JB002372.
- Scott, D.R. & Stevenson, D.J., 1984. Magma solitons, *Geophys. Res. Lett.*, **11**(11), 1161–1164.
- Spiegelman, M., Kelemen, P.B. & Aharonov, E., 2001. Causes and consequences of flow organization during melt transport: the reaction infiltration instability in compactible media, *J. geophys. Res.: Solid Earth*, **106**(B2), 2061–2077.
- Stevenson, D.J., 1989. Spontaneous small-scale melt segregation in partial melts undergoing deformation, *Geophys. Res. Lett.*, **16**(9), 1067–1070.
- Team, T.M.S., 1998. Imaging the deep seismic structure beneath a mid-ocean ridge: the melt experiment, *Science*, **280**(5367), 1215–1218.
- Vardoulakis, I. & Sulem, J., eds, 1995. *Bifurcation Analysis in Geomechanics*, Blankie Acc. and Professional, pp. 150–180.
- Vernon, R. & Paterson, S., 2001. Axial-surface leucosomes in anatectic migmatites, *Tectonophysics*, **335**, 183–192.
- Weinberg, R. & Mark, G., 2008. Magma migration, folding, and disaggregation of migmatites in the Karakoram shear zone, Ladakh, NW India, *Geol. Soc. Am. Bull.*, **120**(7–8), 994–1009.
- Weinberg, R.F., Hasalova, P., Ward, L. & Fanning, C., 2013. Interaction between deformation and magma extraction in migmatites: examples from Kangaroo Island, South Australia, *Geol. Soc. Am. Bull.*, **125**(7–8), 282–1300.

APPENDIX A: ANALYTICAL SOLUTIONS OF EQ. (10)

For integer values of $m < 4$ eq. (9) can be solved analytically, to obtain the solutions listed in the Table A1. For $m = 2, 3$ its closed-form

Table A1. Analytic solutions of eq. (9), for varying rate sensitivity m . Functions $\wp(u, \omega_1, \omega_2)$ and $sn(u, k)$ are the Weierstrass P and Jacobi SN function, respectively (Abramowitz & Stegun 1964) and i is the imaginary number.

Rate sensitivity, m	Solution
$m = 1$	$\sigma' = C_1 e^{\sqrt{\lambda}z} + C_2 e^{-\sqrt{\lambda}z}$
$m = 2$	$\sigma' = \frac{6}{\lambda} \wp(z + C_1, 0, C_2)$
$m = 3$	$\sigma' = \pm C_2 sn \left[\left(\sqrt{\frac{-\lambda}{2}} z + C_1 \right) C_2, i \right]$
Any other m	Num. solution

solution is given in terms of the elliptic Weierstrass P and Jacobi SN functions $\wp(u, \omega_1, \omega_2)$ and $sn(u, k)$, which indeed present singularities (poles) in their solutions [and are correlated with each other, as shown by Abramowitz & Stegun (1964), 18.9.11]. This is not the case when $m = 1$ however, and the effective stress solution is given in terms of stable, hyperbolic trigonometric functions (McKenzie 1984). For all other values of m , eq. (9) has no analytical solution and should be treated numerically.

APPENDIX B: BIFURCATION CRITERION

We retrieve from Abramowitz & Stegun (1964, eq. 16.5.7) that in eq. (12) stress tends to infinity when the argument of sn becomes equal to $iK'(i)$, $K'(i)$ being the complementary complete elliptic integral of the first kind. In our case this would mean that melt channels appear when $\lambda = \lambda_{cr}$, where

$$\lambda_{cr} = -2 \left[\frac{K(i) - K'(i)}{z} \right]^2 cd \left[\frac{K(i) - K'(i)}{z}, i \right]^2, \quad (\text{B1})$$

and $K(i) - K'(i) = 1.31i$ whereas cd is Jacobi's CD function. The expression λ_{cr} of eq. (B1) presents a minimum $\lambda_{cr}^{\min} = 12.7$ at $z = 0.52$, in accordance with the stress profile depicted in Fig. 2(c). For all $\lambda \geq \lambda_{cr}^{\min}$ stress singularities will appear at different z points, as shown in Fig. 2.